Selenium nanoparticles synthesized using an eco-friendly method: Dye decolorization from aqueous solutions, cell viability, antioxidant, and antibacterial effectiveness

Badreah A Al Jahdaly, Najlaa S Al-Radadi, Ghada M.G. Eldin, Albandary Almahri, M.K. K Ahmed, Kamel Shoueir, Izabela Janowska

Selenium nanoparticles synthesized using an eco-friendly method: Dye decolorization from aqueous solutions, cell viability, antioxidant, and antibacterial effectiveness

Badreah A. Al Jahdaly[a] *, Najlaa S. Al-Radadi*[b]*, , Ghada M.G. Eldin*[c]*, Albandary Almahri*[d]*, M. K. Ahmed*[e**]*, Kamel Shoueir*[f,g*]*, Izabela Janowska*[g]

[a] Chemistry Department, Faculty of Applied Science, Umm Al-Qura University, Makkah, Saudi Arabia

[b] Chemistry Department, Faculty of Science, Taibah University, P.O. Box 30002, Al-Madinah Monawara 14177, Saudi Arabia

[c] National organization for drug control and research, P.O. 29

[d] General courses unit, Faculty of Sciences and Arts, King Khalid University, Dhahran Aljanoub, Saudi Arabia.

[e] Physics Department, Faculty of Science, Suez University, Suez, Egypt

[f] Institute of Nanoscience & Nanotechnology, Kafrelsheikh University, 33516, Kafrelsheikh, Egypt

[g] Institut de Chimie et Procédés pour l'Énergie, l'Environnement et la Santé (ICPEES), CNRS UMR 7515-Université de Strasbourg, 25 rue Becquerel 67087 Strasbourg, France

Corresponding author:

***Kamel Shoueir (Ph.D.); kamel_rezk@nano.kfs.edu.eg, rezkshoueir@unistra.fr**

***M. K. Ahmed: e-mail: m.khalaf@sci.suezuni.edu.eg**

Abstract

Selenium nanoparticles (SeNPs) were fabricated using a green microwave technique in the presence of ascorbic acid. The morphological features indicated that the semi-spherical SeNPs with a diameter 8.5-22nm were configured in agglomerated spherical shapes with diameters around 0.47-0.71 μm. Furthermore, the removal of Fuchsin Basic dye from aqueous solutions was investigated upon variation of concentration of SeNPs. The degradation efficiency achieved 100 % for 10 mg of SeNPs after 34 min of visible light irradiation time. The antioxidant activity

was tested via DPPH radical scavenging assay and displayed that the highest scavenging capacity (311.1±15.72 mg/g) was achieved by SeNPs at a concentration of 106.25 mg/mL. Otherwise, the cell viability of SeNPs through human fibroblasts cell lines in-vitro was reduced to be 75.1±3.8 % with nanoparticle concentration around 500 μg/mL. The antibacterial activity was investigated against gram-negative and gram-positive bacteria such as *Escherichia coli (E.coli)*, *Pseudomonas aeruginosa (P. aeruginosa)*, *Klebsiella pneumoniae (K. pneumonia)*, *Staphylococcus aureus (S. aureus)*, and *Bacillus subtilis (B. subtilis)* bacteria after one day of exposure. It was illustrated that SeNPs did not display an activity towards *Staphylococcus aureus*, while it possessed the highest one against *Escherichia coli* with MBC of 50 ± 1.76 μg/mL compared with 26 ± 0.6 μg/mL for the standard antibiotic. These tremendous properties of SeNPs indicate that manipulating multifunctional nanoparticles for versatile wound and skin treatment applications is highly encouraging.

Keywords: SeNPs; ascorbic acid; dye removal; antibacterial; antioxidant.

1. Introduction

Bacterial infection is one of the most problems that might be threatened by the wound healing process [1-4]. The intensive utilization of antibiotics may cause a formation of superbugs, besides antibiotic resistance. Hence, multidrug-resistance could lead to the spreading of lethal bacteria and irremediable diseases. In addition to this, the leakage of antibiotic compounds through water resources may cause serious pollution. Different strategies could be suggested to circumvent these obstacles such as using inorganic nanoparticles (NPs) including copper oxide (CuO-NPs), silver (Ag-NPs), zinc oxide (ZnO-NPs) nano-colloids [5, 6].

One of the materials that could be classified as biocompatible agents is selenium (Se), which is a vital nutrient element for the human body, besides its highly important antioxidant and prooxidant behaviors [6, 7]. Furthermore, it is accepted by the US Food to be utilized for daily dietary supplements [8] and suggested for protection from cardiovascular disease. It plays an important role in biological functions and is a cofactor of numerous antioxidative enzymes such as glutathione peroxidase and thioredoxin reductase, which eliminate free radicals from the body [9]. Se is gathered with at least 25 selenoproteins in the human body that perform various functions: anti-inflammatory, antioxidants, antiviral and anticancer agents [10]. In addition, this element may be involved in the oxidation of thiol groups in the structure of proteins, such as

tyrosine phosphatase and protein kinase C [11]. Also, Se is suggested to inhibit the carcinogenic factors from attacking DNA and thus may prevent tumor growth and angiogenesis [12, 13]. It could be stated that deficiency of Se might reduce the strength of bone besides bone growth. In recent years, interesting studies focused on the synthesize of selenium nanoparticles (SeNPs) increased, as these nanoparticles have interesting biological activity (*in vitro* and *in vivo*), low toxicity, and excellent bioavailability [14]. Therefore, these SeNPs might participate in antioxidant defense systems and play an important role in protecting against oxidative stress [15, 16]. Some researchers have also found that SeNPs are more effective than silver nanoparticles (Ag-NPs) with less toxicity [17, 18]. Besides, the chemical stability of SeNPs is suggested to be higher than that of Ag-NPs. It was hypothesized that SeNPs may inhibit the penetration abilities of coronavirus (COVID-19) through heath cells and thus may abolish their infectious behavior [19]. The unique antimicrobial activity of SeNPs strongly depends on preparation conditions and could be regulated by cellular redox homeostases as the removal of reactive oxidative species (ROS) and the specific enzyme modulation. SeNPs have great potential in cancer chemotherapy to inhibit cancer cell growth and exhibit toxicity of the cell membrane.

Various methodologies were proposed in the literature for the depletion of organic and inorganic toxins from wastewater [20-25]. Some drawbacks hinder these protocols from efficient decolorization owing to extra-chemicals, harsh conditions, cost, toxicity, and low decomposition rate [26]. Photocatalysis's superior technique is based on green sources that use light to create active charge carriers in photosensitive compounds that influence water treatment. Photocatalysis has also some advantages as it is an economic operation due to its ability to be performed under ambient conditions. Also, decaying products are generally harmless and environmentally friendly [27-31].

Spherical Se nanostructures could be synthesized by green synthesis techniques using natural compounds such as ascorbic acid or plant extract and have shown great antimicrobial activity compared with those fabricated via chemical methods [32, 33]. Moreover, the physicochemical properties of SeNPs might be controlled upon the chosen synthesis pathway conditions. The disadvantages of chemical and physical methods include not only high cost and time-consumption but also the use of many toxic chemicals that might be adsorbed on the surface of SeNPs and thus hinder its pharmaceutical and medical utilizations [34]. These obstacles were settled by green synthesis and green approach which is a key factor in the synthesis of SeNPs.

For example, nano-sized SeNPs were prepared from leaves extract of *Withania somnifera* with 50 mM selenious acid [35]. The synthesis of SeNPs using ascorbic acid as a natural compound is valid and nearly exhibited no toxic form like the nanoparticles obtained from chemicals methods [36]. Further, the water-soluble polymer phase might be used as an effective stabilizer in the synthesis of Se colloids [37].

Consequently, the paper designs and describes green and easy handling techniques for the preparation of SeNPs using ascorbic acid as a reducing agent and PVA as a stabilizer. Green synthesized SeNPs could be investigated upon their structure, microstructure, optical and morphological features. Besides, the cell viability in the presence of SeNPs through the human osteoblast cell line (HFB4) was examined. *S. aureus* and *E. coli* as severe gram-positive and gram-negative bacterial strains were selected to evaluate the antimicrobial efficiency of SeNPs. Also, the antioxidant activity using DPPH analysis was tested.

2. Experimental

2.1. Materials, bacterial strains, and mammalian cells

Sodium selenite (Na_2SeO_3, γ-irradiated, lyophilized powder, BioXtra), Polyvinyl alcohol (PVA, 87-90% hydrolyzed, 30. 000 - 70. 000 MW), L-Ascorbic acid (ACS reagent, ≥99%), and methylthiazolyl diphenyltetrazolium bromide (MTT, 98%) were purchased from Sigma- Aldrich, USA. Diphenylpicrylhydrazyl (DPPH) and DMEM-F12 nutrient mixture were purchased from Thermo Fisher Scientific. Other reagents were used as received without pre-treatment.

2.2. Bio-inspired synthesis of SeNPs

The green synthesis of SeNPs was carried out with the chemical reduction of Na_2SeO_3 with ascorbic acid with the aid of polyvinyl alcohol (PVA) as a capping and stabilizing agent. To synthesize the aqueous phase of stabilized SeNPs, sodium selenite solutions (40 mM) and stabilizing agents (as-prepared 0.2% PVA at 90 ^{o}C for 4 hours) were mixed under magnetic stirring at room temperature (R.T) for 15 minutes. After adding the reducing agent, the reaction mixtures were transferred to a Teflon-lined STRT SYNTH microwave reactor (800 W, 50% stirring, temperature 75 ^{o}C, and 1Par). The solution was gradually changed from colorless to orange, confirming the formation of SeNPs. Finally, centrifugation of the solution at 8000 rpm to yield SeNPs was performed. The NPs were washed twice with DDI and twice with absolute

ethanol for purification then drying of the sample in an oven at 50 ^{o}C overnight to obtain a fine black powder.

2.3. Characterization of SeNPs

Ultraviolet absorption spectra of SeNPs diluted in Milli-Q water were performed on a Uv-vis double beam spectrophotometer (Shimadzu, 1800) in the range of $200 \leq 0 \geq 800$ nm. The particle size, shape, and surface morphology were examined by transmission electron microscope (TEM) and scanning electron microscope (SEM), respectively. TEM images were obtained using a JEOL, 2100, Japan, at 120 kV. The colloidal solution of SeNPs was sprayed on a carbon-coated TEM copper grid and dried in the air before the examination. The texture of green fabricated SeNPs was recognized by field emission scanning electron microscopy (SEM, Quanta FEG250). SEM instrument is a pendant with an EDX unit (ZEISS EVO-MA 10, Germany). Fourier transform infrared spectroscopy (FTIR spectra, JASCO, Model no. 4000) was used to illustrate the structure of SeNPs after formation and the range adjusted in the range 4000-500 cm^{-1}.

2.4. Photocatalytic Degradation of Fuchsin Basic dye

The photocatalytic decomposition of Fuchsin Basic dye was carried out in a photoreaction device. Before illumination, the suspension was magnetically stirred for 20 minutes to achieve an equilibrium state from an adsorption-desorption balance in the darkness. Visible light ($420nm < \lambda < 700nm$) was stimulated by irradiation with a 150 W Xe lamp with a 420 λ nm cut filter. To decompose Fuchsin Basic dye, about 5 mg of the SeNPs was added to 20 mL of 15 mg/L as-prepared working dye solution. At regular time intervals, 3 mL of solution was collected after centrifugation at 9000 rpm (SIGMA 2-16P) and the Fuchsin Basic concentration was measured using UV-visible spectroscopy at a maximum absorption wavelength of 546 nm. For a batch catalytic system the evaluation of decomposition (%) was defined as follows [38, 39]:

$$\text{Deg.}(\%) = \left(1 - \frac{C_t}{C_0}\right) \times 100 \qquad (1)$$

As C_o and C_t are the beginning and the final concentration at an irradiation time (t).

2.5. DPPH radical scavenging assay

The antioxidant potency of SeNPs was measured using DPPH (2,2-diphenyl-2-picrylhydrazyl hydrate) analysis according to published elsewhere [40]. Briefly, various concentrations of SeNPs (6.64, 13.28, 26.56, 53.12, and 106.25 mg/mL) were separately treated

with 2 mL of a 0.2 solution mM of DPPH in methanol solvent and mixed well then incubate for 30 minutes under dark. The absorption of the samples was detected at 517 nm using the mentioned before a double beam UV-vis. The antioxidant activity was calculated according to the following equation:

$$\text{Inhibition percentage of DPPH} = \frac{\text{the absorbance of control} - \text{absorbance of sample}}{\text{absorbance of control}} \quad (2)$$

2.6. Cell viability evaluation in the presence of SeNPs

The cell viability in the presence of SeNPs via the human osteoblast cell line (HFB4) was determined using the MTT test [41], which measures the change of yellow dye (3- (4,5-dimethylthiazol-2-yl) -2.5- diphenyltetrazolium bromide) to purple formazan crystal, due to the activity of mitochondrial cytochrome oxidase and succinate dehydrogenase enzymes in the living cells [42]. The cells were cultured in Dulbecco's modified Eagle's medium (DMEM, Gibpco) at 37 °C under 5% CO_2 atmosphere after incubation, the examined cells were seeded with a density of 1×10^4 cells/cm^2 and seeded in 96-well plates. The plates were incubated for one day at 37 °C in a 5% CO_2 atmosphere. The old media was then separated and 200 µm of different concentrations of SeNPs diluted in the medium have been added to HFB4 cells. The final concentrations in the treated wells were 0.0, 100, 200, 300, 400, and 500 ppm. After one day of exposure, cell compatibility was assessed. 20µL solution of MTT in PBS (5 mg /mL) was added to each well and the cells were incubated for another 4 hours at 37 °C in a humidified atmosphere with 5% CO_2. The supernatants were removed, and the formazan crystals were dissolved in 100 µL of DMSO and the optical density was measured at 570 nm. The experiments were validated thrice, and the cytotoxicity was measured by the following equation [43-45]:

$$\text{cell viability} = \frac{\text{The optical density of the sample well}}{\text{The optical density of control well}} \quad (3)$$

2.7. Antibacterial activity of SeNPs

SeNPs were tested toward two different microbes using the cup diffusion method for proving their antimicrobial activity. The types of bacteria are three gram-negative bacteria (*Escherichia coli*, ATCC-8739, *Klebsiella pneumoniae*, ATCC-10031, and *Pseudomonas aeruginosa*, ATCC-27853) and two gram-positive bacteria (*Staphylococcus aureus*, ATCC-6538 and *Bacillus subtilis*, ATCC-6633). The activity was estimated using the agar disc diffusion method. The results were compared to standard antibiotic discs including amoxicillin 30µg,

ceftriaxone 30 µg, cefuroxime 30µg, and norfloxacin 10µg which were purchase from Bioanalyse Company. The antibacterial evaluation protocol included a dissolving of 20 mg of SeNPs into 0.1 mL of sterile saline to obtain a concentration of 200 mg/mL. Next, filter paper discs of 6 mm were immersed to be saturated by the solution of SeNPs and left to dry. Then, the Mueller Hinton agar (MHA) was allowed to be heated reaching the liquefication process, poured next in 10 cm of sterile Petri dishes, covered, and left for 15 min. Using a sterile loop, one colony from each kind of the mentioned bacterial strain could be suspended through sterile saline to be inoculated on the petri dish surface. The discs of investigated SeNPs, with selected concentration, and the standard antibiotic were incubated at 37 ^{o}C for 24 h in the Petri dishes. The experiments were repeated three times to obtain a standard deviation. The concentrations of both SeNPs and slandered antibiotics were presented in µg/mL. The inhibition zone of the compound was recorded against the standard antibiotics including the minimum bactericidal concentration (MBC) and the minimum inhibitory concentration (MIC) values.

3. Results and discussion

3.1. Optical properties

The appearance of scarlet, orange in conjunction with surface Plasmon Resonance (SPR) is a unique optical property for metallic NPs and the color change indicates that the SeNPs are generated (Fig. 1). Ultra-violet visible spectroscopy (UV-vis) was used to monitor the bio-inspired synthesis of SeNPs, the wavelength of which was measured between 200 and 800 nm. The assigned peak at λ = 297 nm is the result of coherent oscillations of free motion of the electrons localized on the one surface of Se particle to the other owing to their SPR. Besides, the color remained stable for two days after a complete reaction, no changes were observed. The obtained results in Fig. 1 undoubtedly confirmed the role of ascorbic acid as a stabilizing and bio-reducing agent. Particularly, SeNPs have properties that depend on size and shape. It was reported that SeNPs have shown a large number of absorption bands near the UV-vis area because of the nature of synthetic protocols and the quantum confinement effect. As an example, Hassanien et al. [27] used Drumstick aqueous extract to produce SeNPs and the SPR band was remarkably at 390 nm. On the other hand, Kirupagaran et al study showed that absorption at 293 nm was a characteristic of SeNPs [46]. Based on this section, the current absorption data are more closed to the previous literature.

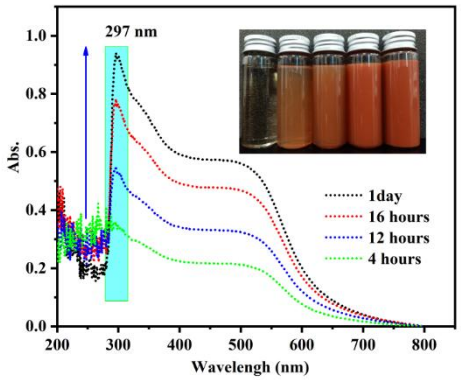

Fig. 1 UV–vis spectra of bio-inspired SeNPs reduced/stabilized by ascorbic acid (inside color changes after SeNPs nanoparticle formation with high stability even after 24 h).

3.2. FTIR spectral investigation

The FTIR spectroscopic illustration was performed to depict the functional groups present in the colloidal form of SeNPs enclosed in the PVA (Fig. 2). In the case of PVA/SeNPs, the absorption band at 3423 cm^{-1} refers to the stretching frequency of –OH groups of the PVA and is also assigned as -OH on the SeNPs surface. The band at 2927 cm^{-1} and the close one at lower cm^{-1} were ascribed to the aliphatic C–H groups along the chain in the structure. Around 1612 cm^{-1} the band corresponds to C=O stretching vibration, while the one observed at 1408 and 1054 cm^{-1} relates to the 2^{nd} $–NH_2$ group and symmetric bending of CH, respectively [47]. The shifted one at 1370 cm^{-1} is attributed to the C-H bending form in the alkanes. FTIR spectral affirms the reduction of Se. The bands at 714 and 555 cm^{-1} refer to the binding of SeNPs with the hydroxyl groups as Se-O as an indication for coordination bonds between Se and ascorbic acid. It should be noted that the reactivity increases with decreasing particle size so that the particles have to be coated in order to avoid particle aggregation. Also, various coating agents were used to stabilizing SeNPs. In this study, Se particles were stabilized by PVA, as shown in the FTIR results.

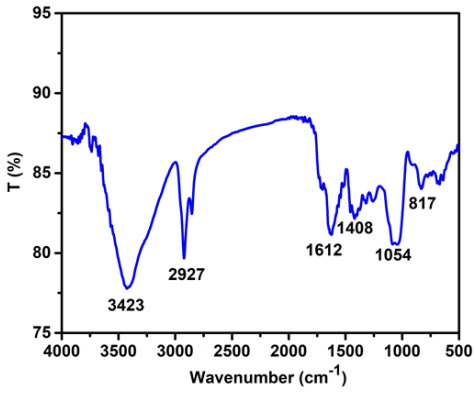

Fig. 2 FT-IR spectra of bio-inspired SeNPs.

3.3. XRD crystallography analysis and thermal stability

X-ray powder crystallography is an important technique to recognize the crystalline phase. As in Fig. 3, the diffraction peaks and their relative planes listed at positions $2\Theta = 22.88^{o}$ (100), 29.28^{o} (101), 40.9^{o} (110), 43.36^{o} (102), 51.12^{o} (112), 55.38^{o} (202), and 60.88^{o} (210), confirming the presence of SeNPs in a crystalline form and accord with JCPDS No. 06-0362. The intense peak located at $2\Theta = 29.28^{o}$ (101), depicted that major orientation occurred to the evaluated facet (101) and also indicated the high purity of SeNPs after preparation. The mean crystallite size could be theoretically measured from the Debye–Scherer equation [48-50]:

$$D = \frac{K\lambda}{\beta \cos\theta} \qquad (4)$$

As K is the Scherer constant (0.9), λ is the wavelength of the X-ray, β is the full width at half point of the XRD peak and θ is the Bragg angle. Thus, the calculated crystallite particle size is around 37 nm. It could be stated that SeNPs were crystallized as hexagonal symmetry with lattice parameters around a=b=4.362 Å and c=4.954 Å.

TGA analysis of the green prepared SeNPs was evaluated and shown in Fig. 3b. The curve trend reveals a weight loss of~ 1.3 % up to 250 ^{o}C, possibly due to unpredictable developments matter (mainly adsorbed with moisture), and so its weight loss seems to be almost complete after about 465 ^{o}C. This might be allocated under the N_2 flowing condition which led to the vaporization of SeNPs.

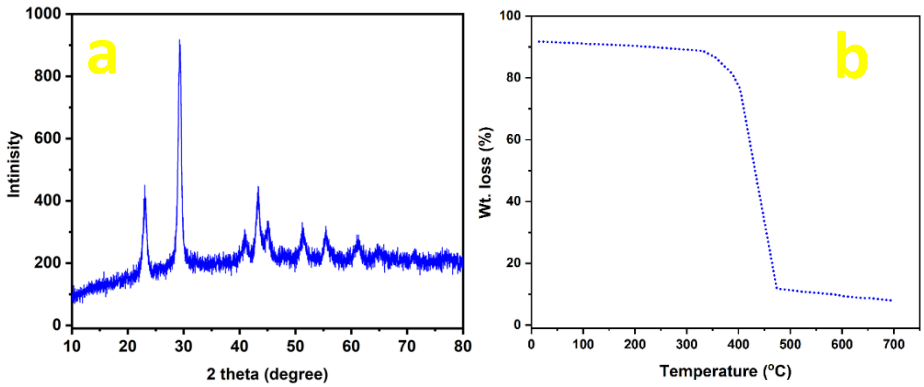

Fig. 3 XRD powder pattern of the crystalline SeNPs (a) and TGA till 700 ^{o}C (b).

3.4. Microstructural and morphological features

SeNPs formation was further investigated using TEM analysis. Fig. 4 shows the particle formation of SeNPs which were configured in semi-spherical shape with homogenous distribution and size about 8.5-22 nm. The TEM at various images of the reaction product shows a mixture of disordered chains and a certain enrichment of the nanostructures. TEM microscopy at various magnifications (Fig. 4a-c) shows a semi-spherical morphology with an adaptable diameter and smooth edges connected with each other. This is similar to other published studies, e.g. Yan, J. K. et al. [51] where SeNPs were prepared via gum Arabic reaching 34 nm as an average size, monodispersed, and spherical shape were also viewed SeNPs obtained with Vinifera showed spherical structures with a size range from 3 to 18 nm [52].

The morphological behavior of SeNPs was studied by SEM. The SEM images of SeNPs were formed with spherical and bulky, which is the predominant form, agreed-upon research reports [53]. The SEM image at two different magnifications (Fig. 4d, e) shows that the SeNPs were made up of spherical shapes with narrow size distribution 0.47-0.71 μm. Moreover, the grains are aggregated over the process owing to the reduction and nucleation growth of the reduced atoms [54]. This returned to the existence of more functional groups such as lignin in an ascorbic acid bind and nucleates selenious acid ions. The more accessible metal ions are apparently involved in fewer nucleation processes, leading to metal agglomeration [33]. Previous reports have shown that spherical and agglomerated NPs have a superior biological activity rather than distorted nanostructured [34, 35].

The correlated surface roughness behavior upon the two mentioned magnifications is shown in Fig. 4f, g. It could be noticed that the roughness average (R_a) is around 16.2 nm, while the maximum height of the roughness (R_t) is 212 nm. The maximum roughness valley depth (R_v) was 162 nm, and the maximum height of the peak roughness (R_p) was 141 nm. This gives information about the nature of notches as well as improving the physical attachment towards the ambient environment [55-57]. The development of surface roughness is hypothesized to support the biocompatibility of fabricated biomaterials, owing to the high chemical affinity of the rough surface to the milieu.

Furthermore, the elemental Se was proved by EDX analysis. The EDX analysis provides a quantitative and qualitative state of elements that may be involved in the formation of nanostructures. Fig. 4h shows a profile of a nanoparticle element that was fabricated using green

ascorbic acid. The elemental Se showed an electronic intense absorption peak at around 1.45 keV with a ratio of 53.4%.

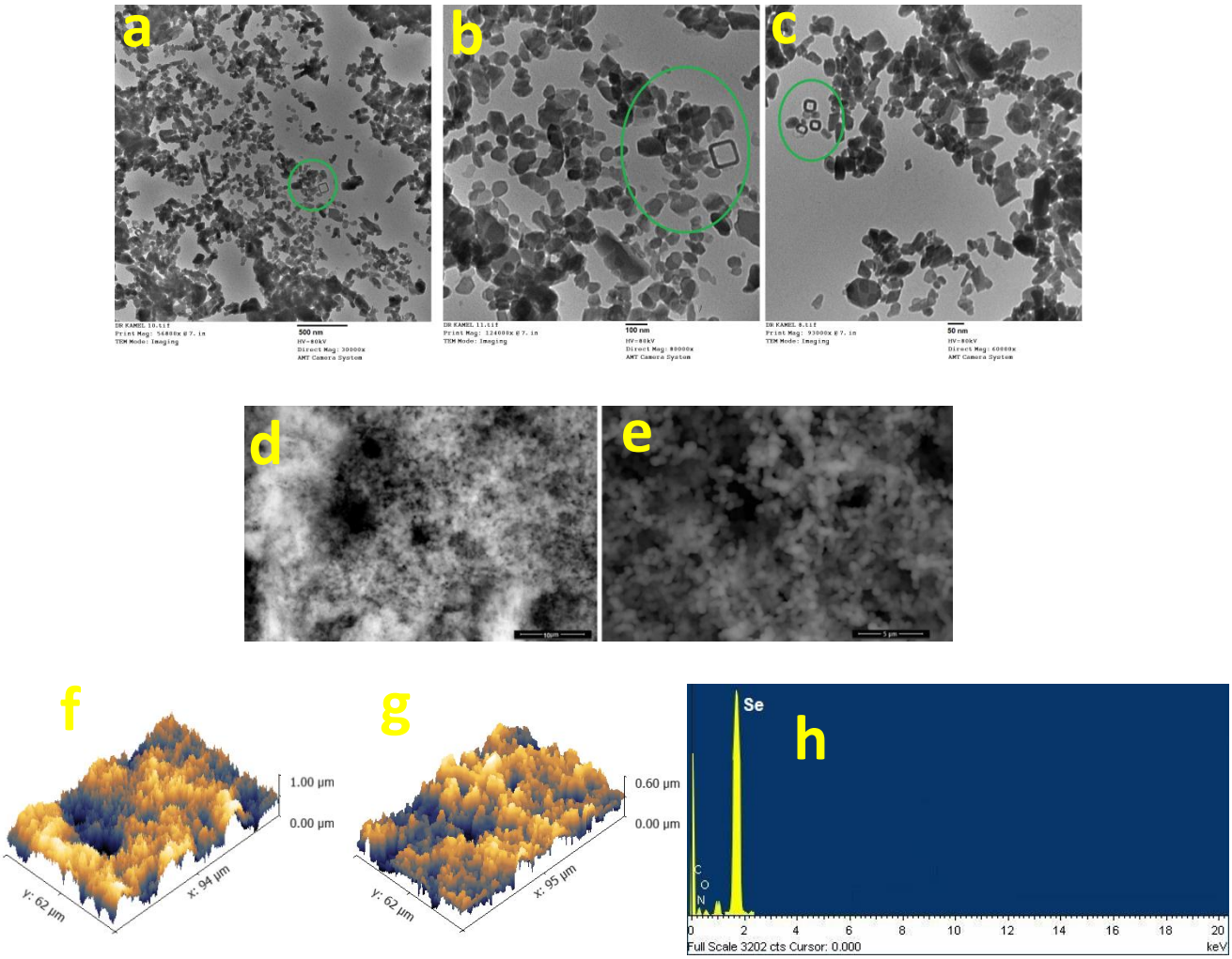

Fig. 4 TEM micrograph images of SeNPs at different magnifications (a, b, c). SEM morphology at 10 and 5µm respectively (d, e), the surface roughness features upon the two previous magnifications (f, g), and EDX profile of bio-inspired prepared SeNPs (h).

3.5. Evaluation of catalytic performance at different dosage

An accepted facile and efficient technique to eliminate organic pollutants from wastewater is a required aspect of environmental technology. Fuchsin Basic dye was completely degraded in this study by SeNPs after some trials. Fig. 5 depicted the UV-vis spectral investigation of Fuchsin Basic at various degradation conditions to attain optimal dye decomposition. There is no adsorption property in the dark state of SeNPs during their dispersion in Fusion Basic. After 20

min from irradiation time, only 70.9% was decomposed when 5mg SeNPs was used (Fig. 5a, e). With increasing the SeNPs dosage, remarkable degradation efficiency was increased to reach 96.4% within 40 min (Fig. 5b, e). The scenario was continued by elevating the dose to 10 mg to achieve complete degradation of Fuchsin Basic within a significant 34 min (Fig. 5c, e). The empirical formula by Langmuir–Hinshelwood (L–H) model was used to better understand the kinetics of the catalyzed reaction in a heterogeneous phase. The stated formula of this model to the apparent pseudo-first-order kinetic given as following [30, 58, 59]:

$$\ln(\frac{C}{C_o}) = -k_{app}t \quad (5)$$

As k_{app} is the pseudo-first-order model constant (min^{-1}), and k_{app} calculated by drawing ln (C/C_o) against irradiated t yields a straight line with a slope of k_{app}. As shown in Fig. 5e and Table 1, all the system obeys pseudo-first-order kinetic, as well as high SeNPs content, holds extra catalytic degradation against the targeted Fuchsin Basic dye. Green preparation possesses small size particles of SeNPs which increased the yield of (•OH) radicals, the major oxidant factor that is required for enhancing the photocatalytic depletion towards pollutants [4, 43].

Table 1. Degradation time, performance, and kinetic parameters for the depletion of Fuchsin Basic

Dose	Degradation time (min)	Degradation (%)	K_{app}	R^2
5 mg	20	70.9	0.063	0.9977
7 mg	40	96.4	0.200	0.9795
10 mg	34	100	0.203	0.9942

3.5.1. Reusability efficiency of SeNPs

The reusability of any catalytic nanomaterials is a major factor in practical application. Thus, six sequential experiments were used to prove the ability of SeNPs to be reused again. To ensure the reusability achievement of SeNPs under different dosage forms (5,7, and 10 mg), the powder form and the photocatalytic system were cleaned thoroughly with continuous water flow and then dried at R.T to prevent any interference. Afterward, under the same photocatalytic conditions, different SeNPs solid contents were treated with new Fusion Basic dye solution for performed to the second use and this step was repeated six times. Fig. 5f showed that the bio-inspired SeNPs exhibited superior stability with a very limited loss in the efficiency of 62.5 %, 92.1 %, and 96.1 % for 5, 7, and 10 mg, respectively. These data possesses that SeNPs have adequate stability,

presenting only tiny decay in the degradation performance regarded the original degradation and can be used as a suitable recyclable nanocatalyst [60, 61].

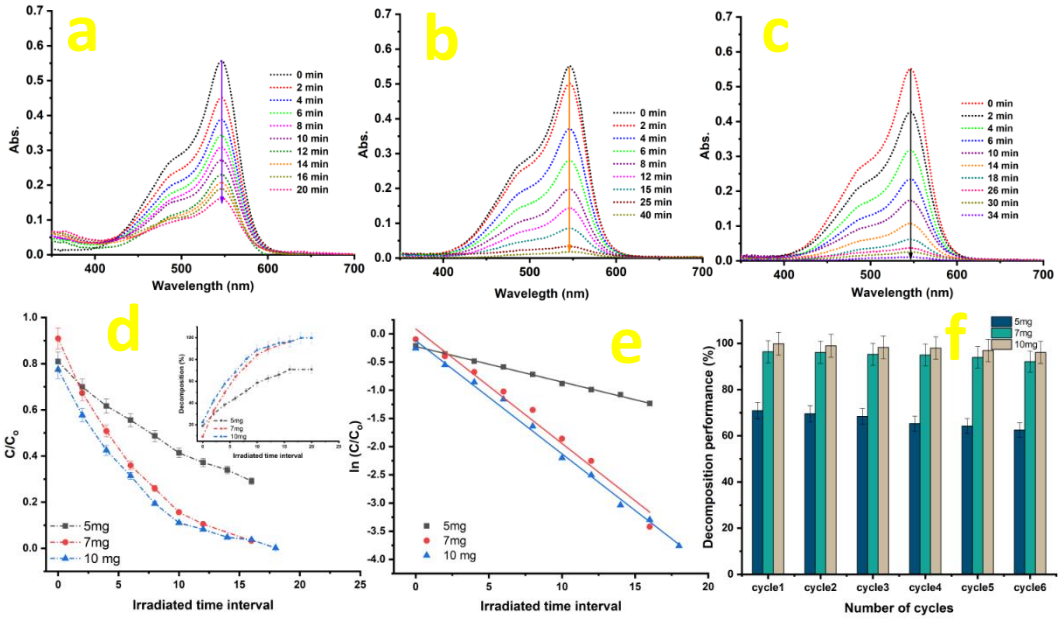

Fig. 5 UV-vis adsorption degradation of (a) 5 mg, (b) 7 mg, (c) 10 mg SeNPs, (d) photodecomposition of Fuchsin Basin (inset, decomposition %), (e) kinetics comparison at different dosage, and reusability performance (f).

The proposed mechanism for the degradation of the Fuchsin Basin dye is presented in Fig 6. In the beginning, SeNPs adsorbs Fuchsin Basin dye ions, then after, initiation of the degradation by UV-lamp led to the stimulation of photo-regenerated electrons in the C.B area. Consequently, the photo-regenerated electrons in the V.B were easily migrating to the surface of SeNPs to trigger redox reactions [62-64]. The holes reacted with water or HO^-, which rapidly adsorbed onto the SeNPs surface to form OH^* radicals. The superoxide oxyanion radicals O_2^{-*} being observed by the reacting of electrons e^- with O_2, and O_2^{-*} reacted with h^+ to promote peroxide radicals of HOO^*. All these powerfully active species OH^*, O_2^{-*}, and h^+deplete Fuchsin Basin dye molecules into H_2O, CO_2, and minerals (colorless products) through a series of redox reactions [65-67].

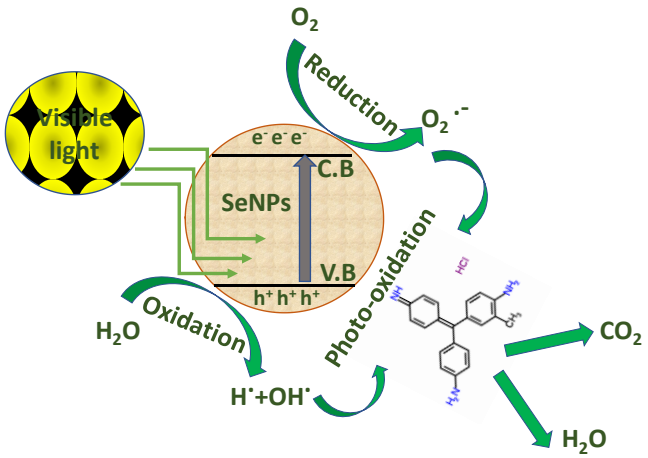

Fig. 6 Scheme postulated mechanism formation of photodecomposition of Fuchsin Basic dye by the aid of SeNPs.

3.6. In vitro antioxidant activity

The antioxidant potency of SeNPs could be examined using the DPPH radical scavenging assay. As obvious in Fig. 7, the activity of DPPH radical scavenging increases with increasing the concentration of SeNPs. It could be illustrated that when SeNPs concentration grew from 6.64 to 106.25 mg/mL, the scavenging capacity increased significantly from 45.55±6.18 reaching 311.1±15.72 mg/g. This high ability of SeNPs to deactivate these free radicles might be assigned to the dispersibility of nanoparticles through the media owing to the small particle size, besides the high chemical activity of SeNPs [68]. The oxygen-releasing antioxidant may enhance the efficiency of cells to be proliferated, migrate, grow, and spread, and thus develop the healing process. Hence, excellent potency to collect free radicals from physiological media could inhibit cancer cell initiation, and consequently progression of care health procedures [69].

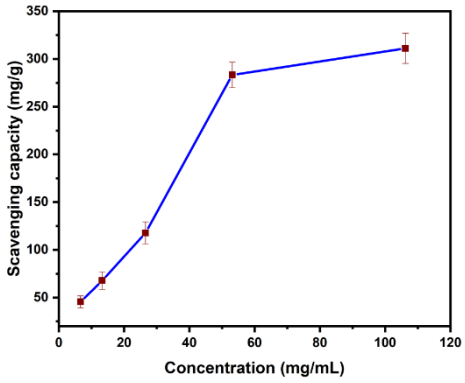

Fig. 7 The scavenging activity upon DPPH radicals for SeNPs; the standard deviation is included from three times of repetitions.

3.7. In-vitro cell viability in the presence of SeNPs

The in-vitro cytotoxicity of the SeNPs was performed on the human fibroblast cell line (HFB4). This has been carried out to understand the possible cytotoxic activity of different contents of SeNPs. As obvious in Fig. 8, it could be shown that by raising the content of SeNPs, the cell viability was reduced significantly. It started from 97.3±3.1 % for the untreated cell line (control one) and decreased reaching 75.1±3.8 % for the highest content of SeNPs, which was around 500 µg/mL. The high effect of SeNPs towards cells is assigned to the release of nanoparticle colloids through the cell culture, and thus may facilitate ROS to have interacted with cell membranes. This scenario might be hypothesized to degenerate life cells and cause a high ratio of mortality for these cells. Moreover, it could be stated that the cytotoxicity of SeNPs depends strongly on their particle size, distribution, and crystallinity [70]. This is because low crystalline nanoparticles tend to have high degradation rates and thus leads to an increase in the effective content of those nanoparticles. Therefore, controlling toxic behavior could be done deeply via preparation conditions.

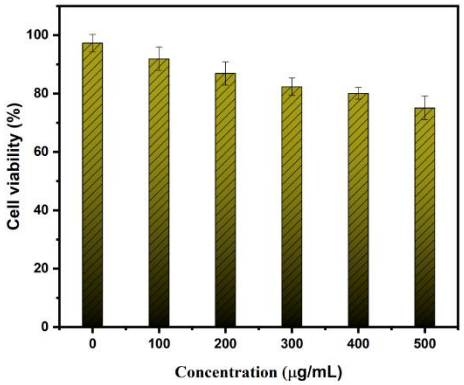

Fig. 8 Cell viability ratio in the presence of SeNPs that was cultivated through HFB4 cell lines for 3 days in-vitro.

3.8. Antibacterial activity

The potency of the SeNPs to degenerate bacterial cells is a vital requirement for numerous biomedical utilizations. Therefore, the antibacterial activity of SeNPs was tested in vitro study against different specific strains including both gram-negative (*E. coli*, *P. aeruginosa*, and *K. pneumoniae*) and gram-positive (*S. aureus and B. subtilis*) bacteria via the disc diffusion method

compared with standard antibiotic discs. Fig. 9 shows the antibacterial activity, whereas Table 2 reports the measured inhibition zone for these strains. It could be noticed that the SeNPs do not display any activity towards S. aureus compared with the standard antibiotic. The minimum bactericidal concentration (MBC) represents the lowest content of SeNPs that cause complete death for the bacterial colony, which reached around 23±0.07 μg/mL compared with 34 ± 0.16 μg/mL for the standard antibiotic. Likewise, the minimum inhibitory concentration (MIC), which indicates the lowest concentration of SeNPs that can inhibit the growth of bacteria after an overnight of incubation achieved about 12.5 ± 1.3 μg/mL for *B. subtilis*. On the other hand, MBC increased for *E. coli* to be about 50 ± 1.76 μg/mL, while MIC was around 11 ± 0.08 μg/mL. It might be noticed that the SeNPs possess higher activity towards gram-negative type bacteria than gram-positive ones. This behavior is assigned to the cellular composition for both types. The destruction of the cytoplasmic membrane and the appearance of various cytoplasmic biomolecules, such as proteins, amino acids, and carbohydrates, are the main causes of bacterial cell death due to exposure to NPs [71, 72]. It was reported that the bactericidal activity of SeNPs is associated with the triggering of reactive oxygen species abundance, which leads to significant oxidative stress and, in turn, leads to lipid peroxidation and oxidation of proteins and DNA damage [73]. In addition to this, the negative charges that could be detected on the protein walls of bacteria may provoke the interaction with ionic species created owing to the presence of SeNPs. The mechanism of bacterial mortality due to the interaction with SeNPs is illustrated in Fig. 10.

Table 2 Antibacterial activity represented by inhibition zone for SeNPs including Minimum inhibitory concentration (MIC) assays and minimum bactericidal concentration (MBC) values against gram-negative (*E. coli, P. aeruginosa and K. pneumoniae*) and gram-positive (*S. aureus* and *B. subtilis*) bacteria (μg/mL), whereas (the Inhibition zone < 10 mm is considered non-sensitive (NS)).

Compound	***S. aureus***		***B. subtilis***		***K. pneumoniae***		***E. coli***		***P. aeruginosa***	
	MBC	**MIC**	**MBC**	**MIC**	**MBC**	**MIC**	**MBC**	**MIC**	**MBC**	**MIC**
SeNPs	NS	---	23 ± 0.07	12.5 ± 1.3	33 ± 0.25	25 ± 1.5	50 ± 1.76	11 ± 0.08	35 ± 1.82	12.5 ± 0.92
Standard antibiotic	21 ± 0.09	---	34 ± 0.16	---	35 ± 0.7	---	26 ± 0.6	---	35 ± 0.8	---

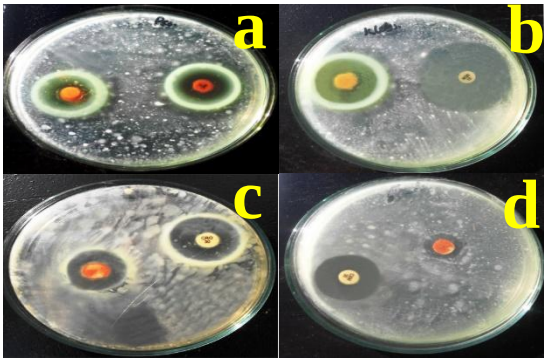

Fig. 9 The inhibition zone of SeNPs against different bacterial strains; where the colored disk represented SeNPs and the other disk represented the standard antibiotic disc; *B. subtilis* (a), *K. pneumoniae* (b), *S. aureus* (c), and *E. coli* (d).

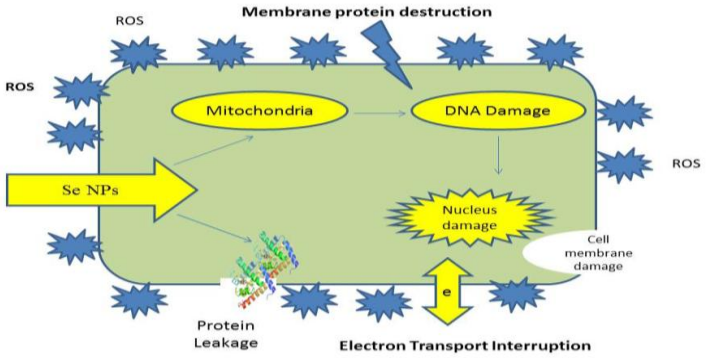

Fig. 10 Hypothesized mechanism of antibacterial activity of synthesized SeNPs.

4. Conclusion

Selenium nanoparticles (SeNPs) were synthesized using an eco-friendly method. The obtained nanoparticles were characterized and examined for antioxidant and antibacterial activity, as well as dye removal from aqueous solutions. The crystallite size of the as-synthesized SeNPs was around 37 nm, while the lattice parameters for the hexagonal symmetry were a=b=4.362 Å and c=4.954 Å. The TEM investigation indicated that SeNPs were formed in monodisperse and semi-spherical with dimensions around 19 to 31 nm. The morphological investigation by SEM illustrated that SeNPs were formed in agglomerated spherical shapes with diameters around 0.47-0.71 µm. The surface roughness was examined, and a roughness average (R_a) was about 16.2 nm. Furthermore, the effectiveness of Fuchsin Basic dye removal by different contents of SeNPs

was tested, and the degradation efficiency reached 100 % for 10 mg of SeNPs after 18 min of irradiation time. The antioxidant activity was examined using DPPH radical scavenging and showed that the highest scavenging capacity (311.1±15.72 mg/g) was achieved by SeNPs with a concentration of 106.25 mg/mL. The antibacterial activity was hard on *E. coli*, *P. aeruginosa*, *K. pneumoniae*, *S. aureus*, and *B. subtilis*. While SeNPs did not show activity towards *S. aureus*, it showed the highest one against *E. coli* with MBC of 50 ± 1.76 μg/mL compared with 26 ± 0.6 μg/mL for the standard antibiotic. This high potency of SeNPs encourages their usage in numerous biomedical applications.

References

[1] Y. Zou, R. Xie, E. Hu, P. Qian, B. Lu, G. Lan, F. Lu, Protein-reduced gold nanoparticles mixed with gentamicin sulfate and loaded into konjac/gelatin sponge heal wounds and kill drug-resistant bacteria, International journal of biological macromolecules 148 (2020) 921-931.

[2] A.A. Menazea, M.K. Ahmed, Wound healing activity of Chitosan/Polyvinyl Alcohol embedded by gold nanoparticles prepared by nanosecond laser ablation, Journal of Molecular Structure (2020) 128401.

[3] A.A. Menazea, M.K. Ahmed, Nanosecond laser ablation assisted the enhancement of antibacterial activity of copper oxide nano particles embedded though Polyethylene Oxide/Polyvinyl pyrrolidone blend matrix, Radiation Physics and Chemistry 174 (2020) 108911.

[4] A.A. Menazea, M.K. Ahmed, Silver and copper oxide nanoparticles-decorated graphene oxide via pulsed laser ablation technique: Preparation, characterization, and photoactivated antibacterial activity, Nano-Structures & Nano-Objects 22 (2020) 100464.

[5] A.A. Menazea, M.K. Ahmed, Synthesis and antibacterial activity of graphene oxide decorated by silver and copper oxide nanoparticles, Journal of Molecular Structure 1218 (2020) 128536.

[6] A.A. Menazea, S.A. Abdelbadie, M.K. Ahmed, Manipulation of AgNPs coated on selenium/carbonated hydroxyapatite/ε-polycaprolactone nano-fibrous via pulsed laser deposition for wound healing applications, Applied Surface Science 508 (2020) 145299.

[7] Z. Qiu, Q. Tian, T. Zhang, D. Yang, F. Qiu, Fabrication of dynamic zero-valent iron/MnO_2 nanowire membrane for efficient and recyclable selenium separation, Separation and Purification Technology 230 (2020) 115847.

[8] Y. Wang, W. He, H. Hao, J. Wu, N. Qin, Eggshell derived Se-doped HA nanorods for enhanced antitumor effect and curcumin delivery, Journal of Sol-Gel Science and Technology 87(3) (2018) 600-607.
[9] A. Caglayan, D.C. Katlan, Z.S. Tuncer, K. Yüce, Evaluation of trace elements associated with antioxidant enzymes in blood of primary epithelial ovarian cancer patients, Journal of Trace Elements in Medicine and Biology 52 (2019) 254-262.
[10] R. Alhasan, A. Kharma, P. Leroy, C. Jacob, C. Gaucher, Selenium donors at the junction of inflammatory diseases, Current pharmaceutical design 25(15) (2019) 1707-1716.
[11] M. Farina, M. Aschner, Glutathione antioxidant system and methylmercury-induced neurotoxicity: an intriguing interplay, Biochimica et Biophysica Acta (BBA)-General Subjects 1863(12) (2019) 129285.
[12] M.S. Ali, R.M. Hussein, M.A. Kandeil, The Pro-Oxidant, Apoptotic and Anti-Angiogenic Effects of Selenium Supplementation on Colorectal Tumors Induced by 1, 2-Dimethylhydrazine in BALB/C Mice, Reports of Biochemistry & Molecular Biology 8(3) (2019) 216.
[13] A. Shrivastava, L.M. Aggarwal, S.P. Mishra, H.D. Khanna, U.P. Shahi, S. Pradhan, Free radicals and antioxidants in normal versus cancerous cells—An overview, Indian Journal of Biochemistry and Biophysics (IJBB) 56(1) (2019) 7-19.
[14] P. Adadi, N.V. Barakova, K.Y. Muravyov, E.F. Krivoshapkina, Designing selenium functional foods and beverages: A review, Food research international 120 (2019) 708-725.
[15] S. Rao, Y. Lin, Y. Du, L. He, G. Huang, B. Chen, T. Chen, Designing multifunctionalized selenium nanoparticles to reverse oxidative stress-induced spinal cord injury by attenuating ROS overproduction and mitochondria dysfunction, Journal of Materials Chemistry B 7(16) (2019) 2648-2656.
[16] K.A. Amin, K.S. Hashem, F.S. Alshehri, S.T. Awad, M.S. Hassan, Antioxidant and hepatoprotective efficiency of selenium nanoparticles against acetaminophen-induced hepatic damage, Biological trace element research 175(1) (2017) 136-145.
[17] A.T.A. Ibrahim, Toxicological impact of green synthesized Silver nanoparticles and protective role of different Selenium type on Oreochromis niloticus: Hematological and biochemical response, Journal of Trace Elements in Medicine and Biology (2020) 126507.
[18] A.K. Mittal, K. Thanki, S. Jain, U.C. Banerjee, Comparative studies of anticancer and antimicrobial potential of bioinspired silver and silver-selenium nanoparticles, Applied Nanomedicine 1(1) (2016) 1-6.

[19] M. Kieliszek, B. Lipinski, Selenium supplementation in the prevention of coronavirus infections (COVID-19), Medical hypotheses 143 (2020) 109878.
[20] J. Wang, Z. Wang, C.L. Vieira, J.M. Wolfson, G. Pingtian, S. Huang, Review on the treatment of organic pollutants in water by ultrasonic technology, Ultrasonics sonochemistry 55 (2019) 273-278.
[21] X. Li, G.-z. Wang, W.-g. Li, P. Wang, C.-y. Su, Adsorption of acid and basic dyes by sludge-based activated carbon: Isotherm and kinetic studies, Journal of Central South University 22(1) (2015) 103-113.
[22] G. Bayramoglu, A. Akbulut, G. Liman, M.Y. Arica, Removal of metal complexed azo dyes from aqueous solution using tris (2-aminoethyl) amine ligand modified magnetic p (GMA-EGDMA) cationic resin: Adsorption, isotherm and kinetic studies, Chemical Engineering Research and Design 124 (2017) 85-97.
[23] M. Naushad, A.A. Alqadami, Z.A. AlOthman, I.H. Alsohaimi, M.S. Algamdi, A.M. Aldawsari, Adsorption kinetics, isotherm and reusability studies for the removal of cationic dye from aqueous medium using arginine modified activated carbon, Journal of Molecular Liquids 293 (2019) 111442.
[24] K.R. Shoueir, A. Sarhan, A.M. Atta, M.A. Akl, Adsorption studies of Cu^{2+} onto poly (vinyl alcohol)/poly (acrylamide-co-N-isopropylacrylamide) core–shell nanogels synthesized through surfactant-free emulsion polymerization, Separation Science and Technology 51(10) (2016) 1605-1617.
[25] K.R. Shoueir, Green microwave synthesis of functionalized chitosan with robust adsorption capacities for Cr (VI) and/or RHB in complex aqueous solutions, Environmental Science and Pollution Research (2020) 1-12.
[26] H. Anwer, A. Mahmood, J. Lee, K.-H. Kim, J.-W. Park, A.C. Yip, Photocatalysts for degradation of dyes in industrial effluents: Opportunities and challenges, Nano Research 12(5) (2019) 955-972.
[27] R. Hassanien, A.A. Abed- Elmageed, D.Z. Husein, Eco- Friendly Approach to Synthesize Selenium Nanoparticles: Photocatalytic Degradation of Sunset Yellow Azo Dye and Anticancer Activity, ChemistrySelect 4(31) (2019) 9018-9026.
[28] M.N. Zafar, Q. Dar, F. Nawaz, M.N. Zafar, M. Iqbal, M.F. Nazar, Effective adsorptive removal of azo dyes over spherical ZnO nanoparticles, Journal of Materials Research and Technology 8(1) (2019) 713-725.

[29] M. Naushad, G. Sharma, Z.A. Alothman, Photodegradation of toxic dye using Gum Arabic-crosslinked-poly (acrylamide)/Ni(OH)$_2$/FeOOH nanocomposites hydrogel, Journal of Cleaner Production 241 (2019) 118263.

[30] M.F. Abdelbar, H.S. El-Sheshtawy, K.R. Shoueir, I. El-Mehasseb, E.-Zeiny M. Ebeid, M. El-Kemary, Halogen bond triggered aggregation induced emission in an iodinated cyanine dye for ultra sensitive detection of Ag nanoparticles in tap water and agricultural wastewater, RSC Advances 8(43) (2018) 24617-24626.

[31] H.S. El-Sheshtawy, K.R. Shouir, M. El-Kemary, Activated H_2O_2 on Ag/SiO_2–SrWO4 surface for enhanced dark and visible-light removal of methylene blue and p-nitrophenol, Journal of Alloys and Compounds (2020) 155848.

[32] G. Zhang, L. Zhou, D. Cai, Z. Wu, Anion-responsive carbon nanosystem for controlling selenium fertilizer release and improving selenium utilization efficiency in vegetables, Carbon 129 (2018) 711-719.

[33] X. Wang, D. Zhang, X. Pan, D.J. Lee, F.A. Al-Misned, M.G. Mortuza, G.M. Gadd, Aerobic and anaerobic biosynthesis of nano-selenium for remediation of mercury contaminated soil, Chemosphere 170 (2017) 266-273.

[34] P.G. Jamkhande, N.W. Ghule, A.H. Bamer, M.G. Kalaskar, Metal nanoparticles synthesis: An overview on methods of preparation, advantages and disadvantages, and applications, Journal of Drug Delivery Science and Technology (2019) 101174.

[35] V. Alagesan, S. Venugopal, Green synthesis of selenium nanoparticle using leaves extract of withania somnifera and its biological applications and photocatalytic activities, Bionanoscience 9(1) (2019) 105-116.

[36] M. Korany, B. Mahmoud, S.M. Ayoub, T.M. Sakr, S.A. Ahmed, Synthesis and radiolabeling of vitamin C- stabilized selenium nanoparticles as a promising approach in diagnosis of solid tumors, Journal of Radioanalytical and Nuclear Chemistry 325 (2020) 237-244.

[37] P.A. Tran, N. O'Brien-Simpson, J.A. Palmer, N. Bock, E.C. Reynolds, T.J. Webster, A. Deva, W.A. Morrison, A.J. O'connor, Selenium nanoparticles as anti-infective implant coatings for trauma orthopedics against methicillin-resistant Staphylococcus aureus and epidermidis: in vitro and in vivo assessment, International journal of nanomedicine 14 (2019) 4613.

[38] A. Salama, K.R. Shoueir, H.A. Aljohani, Preparation of sustainable nanocomposite as new adsorbent for dyes removal, Fibers and Polymers 18(9) (2017) 1825-1830.

[39] K.R. Shoueir, M.A. Akl, A.A. Sarhan, A.M. Atta, New core@shell nanogel based 2-acrylamido-2-methyl-1-propane sulfonic acid for preconcentration of Pb(II) from various water samples, Applied Water Science 7(7) (2016) 3729-3740.

[40] S. Boroumand, M. Safari, E. Shaabani, M. Shirzad, R. Faridi-Majidi, Selenium nanoparticles: synthesis, characterization and study of their cytotoxicity, antioxidant and antibacterial activity, Materials Research Express 6(8) (2019) 0850d8.

[41] N. El-Desouky, K. R. Shoueir, I. El-Mehasseb, M. El-Kemary, Bio-inspired green manufacturing of plasmonic silver nanoparticles/Degussa using Banana Waste Peduncles: Photocatalytic, antimicrobial, and cytotoxicity evaluation, 10 (2021) 671-686.

[42] V. Ruiz-Torres, C. Rodríguez-Pérez, M. Herranz-López, B. Martín-García, A.-M. Gómez-Caravaca, D. Arráez-Román, A. Segura-Carretero, E. Barrajón-Catalán, V. Micol, Marine Invertebrate Extracts Induce Colon Cancer Cell Death via ROS-Mediated DNA Oxidative Damage and Mitochondrial Impairment, Biomolecules 9(12) (2019) 771.

[43] S.F. Mansour, R. Al-Wafi, M.K. Ahmed, S. Wageh, Microstructural, morphological behavior and removal of Cr(VI) and Se(IV) from aqueous solutions by magnetite nanoparticles/PVA and cellulose acetate nanofibers, Applied Physics A 126(3) (2020).

[44] R. Al-Wafi, S.F. Mansour, M.K. Ahmed, Mechanical, microstructural properties and cell adhesion of Sr/Se-hydroxyapatite/graphene/polycaprolactone nanofibers, Journal of Thermoplastic Composite Materials (2020) 089270572091278.

[45] M.K. Ahmed, A.A. Menazea, A.M. Abdelghany, Blend biopolymeric nanofibrous scaffolds of cellulose acetate/epsilon-polycaprolactone containing metallic nanoparticles prepared by laser ablation for wound disinfection applications, International journal of biological macromolecules 155 (2020) 636-644.

[46] R. Kirupagaran, A. Saritha, S. Bhuvaneswari, Journal of Nanoscience and Technology, Journal of Nanoscience and Technology 2(5) (2016) 224-226.

[47] W. Yanhua, H. Hao, Y. Li, S. Zhang, Selenium-substituted hydroxyapatite nanoparticles and their in vivo antitumor effect on hepatocellular carcinoma, Colloids and surfaces. B, Biointerfaces 140 (2016) 297-306.

[48] K. Shoueir, M.K. Ahmed, S.A. Abdel Gaber, M. El-Kemary, Thallium and selenite doped carbonated hydroxyapatite: Microstructural features and anticancer activity assessment against human lung carcinoma, Ceramics International 46(4) (2020) 5201-5212.

[49] S.F. Mansour, S.I. El-dek, M. Ismail, M.K. Ahmed, Structure and cell viability of Pd substituted hydroxyapatite nano particles, Biomedical Physics & Engineering Express 4(4) (2018) 045008.
[50] M.K. Ahmed, S.F. Mansour, M.S. Mostafa, R. Darwesh, S.I. El-dek, Structural, mechanical and thermal features of Bi and Sr co-substituted hydroxyapatite, Journal of Materials Science 54(3) (2018) 1977-1991.
[51] W.-Y. Qiu, Y.-Y. Wang, M. Wang, J.-K. Yan, Construction, stability, and enhanced antioxidant activity of pectin-decorated selenium nanoparticles, Colloids and Surfaces B: Biointerfaces 170 (2018) 692-700.
[52] S. Skalickova, V. Milosavljevic, K. Cihalova, P. Horky, L. Richtera, V. Adam, Selenium nanoparticles as a nutritional supplement, Nutrition 33 (2017) 83-90.
[53] S. Menon, S.D. KS, H. Agarwal, V.K. Shanmugam, Efficacy of Biogenic Selenium Nanoparticles from an extract of ginger towards evaluation on anti-microbial and anti-oxidant activities, Colloid and Interface Science Communications 29 (2019) 1-8.
[54] Y. Wang, J. Wang, H. Hao, M. Cai, S. Wang, J. Ma, Y. Li, C. Mao, S. Zhang, In Vitro and in Vivo Mechanism of Bone Tumor Inhibition by Selenium-Doped Bone Mineral Nanoparticles, ACS nano 10(11) (2016) 9927-9937.
[55] M.K. Ahmed, S.F. Mansour, R. Al-Wafi, A. Anter, Composition and design of nanofibrous scaffolds of Mg/Se- hydroxyapatite/graphene oxide @ ε-polycaprolactone for wound healing applications, Journal of Materials Research and Technology 9(4) (2020) 7472-7485.
[56] M.K. Ahmed, S.F. Mansour, R. Al-Wafi, M. Afifi, V. Uskokovic, Gold as a dopant in selenium-containing carbonated hydroxyapatite fillers of nanofibrous epsilon-polycaprolactone scaffolds for tissue engineering, International journal of pharmaceutics 577 (2020) 118950.
[57] M.K. Ahmed, S.F. Mansour, R. Al-Wafi, Nanofibrous scaffolds of epsilon-polycaprolactone containing Sr/Se-hydroxyapatite/ graphene oxide for tissue engineering applications, Biomedical materials (2020).
[58] R.E. Abou-Zeid, M.A. Diab, S.A.A. Mohamed, A. Salama, H.A. Aljohani, K.R. Shoueir, Surfactant-Assisted Poly(lactic acid)/Cellulose Nanocrystal Bionanocomposite for Potential Application in Paper Coating, Journal of Renewable Materials 6(4) (2018) 394-401.
[59] K.R. Shoueir, A.M. Atta, A.A. Sarhan, M.A. Akl, Synthesis of monodisperse core shell PVA@P(AMPS-co-NIPAm) nanogels structured for pre-concentration of Fe(III) ions, Environmental technology 38(8) (2017) 967-978.

[60] K. Shoeir, S. Kandil, H. El-hosainy, M. El-Kemary, Tailoring the surface reactivity of plasmonic Au@TiO_2 photocatalyst bio-based chitosan fiber towards cleaner of harmful water pollutants under visible-light irradiation, Journal of Cleaner Production 230 (2019) 383-393.
[61] R. El-Shabasy, N. Yosri, H. El-Seedi, K. Shoeir, M. El-Kemary, A green synthetic approach using chili plant supported Ag/Ag_2O@P25 heterostructure with enhanced photocatalytic properties under solar irradiation, Optik 192 (2019) 162943.
[62] S. Sathiyavimal, S. Vasantharaj, T. Kaliannan, A. Pugazhendhi, Eco-biocompatibility of chitosan coated biosynthesized copper oxide nanocomposite for enhanced industrial (Azo) dye removal from aqueous solution and antibacterial properties, Carbohydrate Polymers 241 (2020) 116243.
[63] N.M. Mahmoodi, M. Oveisi, A. Taghizadeh, M. Taghizadeh, Synthesis of pearl necklace-like ZIF-8@chitosan/PVA nanofiber with synergistic effect for recycling aqueous dye removal, Carbohydr Polym 227 (2020) 115364.
[64] S.M. Hosseini, M. Shahrousvand, S. Shojaei, H.A. Khonakdar, A. Asefnejad, V. Goodarzi, Preparation of superabsorbent eco-friendly semi-interpenetrating network based on cross-linked poly acrylic acid/xanthan gum/graphene oxide (PAA/XG/GO): Characterization and dye removal ability, International journal of biological macromolecules 152 (2020) 884-893.
[65] T. de Figueiredo Neves, N. Barticiotto Dalarme, P.M.M. da Silva, R. Landers, C. Siqueira Franco Picone, P. Prediger, Novel magnetic chitosan/quaternary ammonium salt graphene oxide composite applied to dye removal, Journal of Environmental Chemical Engineering 8(4) (2020) 103820.
[66] M. Dadashi Firouzjaei, F. Akbari Afkhami, M. Rabbani Esfahani, C.H. Turner, S. Nejati, Experimental and molecular dynamics study on dye removal from water by a graphene oxide-copper-metal organic framework nanocomposite, Journal of Water Process Engineering 34 (2020) 101180.
[67] J. Bhadra, H. Parangusan, A. Popelka, M. Lehocky, P. Humpolicek, N. Al-Thani, Electrospun Polystyrene/PANI-Ag fibers for organic dye removal and antibacterial application, Journal of Environmental Chemical Engineering 8(3) (2020) 103746.
[68] X. Yao, H. Hu, Y. Qin, J. Liu, Development of antioxidant, antimicrobial and ammonia-sensitive films based on quaternary ammonium chitosan, polyvinyl alcohol and betalains-rich cactus pears (Opuntia ficus-indica) extract, Food Hydrocolloids 106 (2020) 105896.

[69] A.A. El- Bindary, E.A. Toson, K.R. Shoueir, H.A. Aljohani, M.M. Abo- Ser, Metal–organic frameworks as efficient materials for drug delivery: Synthesis, characterization, antioxidant, anticancer, antibacterial and molecular docking investigation, Applied Organometallic Chemistry (2020) e5905.

[70] V.L.C. Tan, A. Hinchman, R. Williams, P.A. Tran, K. Fox, Nanostructured biomedical selenium at the biological interface (Review), Biointerphases 13(6) (2018) 06D301.

[71] P. Makvandi, C.y. Wang, E.N. Zare, A. Borzacchiello, L.n. Niu, F.R. Tay, Metal- Based Nanomaterials in Biomedical Applications: Antimicrobial Activity and Cytotoxicity Aspects, Advanced Functional Materials (2020) 1910021.

[72] M.F. Abdelbar, R.S. Shams, O.M. Morsy, M.A. Hady, K. Shoueir, R. Abdelmonem, Highly ordered functionalized mesoporous silicate nanoparticles reinforced poly (lactic acid) gatekeeper surface for infection treatment, International Journal of Biological Macromolecules 156 (2020) 858-868.

[73] A. Nastulyavichus, S. Kudryashov, N. Smirnov, I. Saraeva, A. Rudenko, E. Tolordava, A. Ionin, Y. Romanova, D. Zayarny, Antibacterial coatings of Se and Si nanoparticles, Applied Surface Science 469 (2019) 220-225.